Heliyon 10 (2024) e36483

Contents lists available at ScienceDirect

Heliyon

journal homepage: www.cell.com/heliyon

Research article

Navitoclax safety, tolerability, and effect on biomarkers of senescence and neurodegeneration in aged nonhuman primates

Edward F. Greenberg [a,*], Martin J. Voorbach [a], Alexandra Smith [a], David R. Reuter [a], Yuchuan Zhuang [a], Ji-Quan Wang [a], Dustin W. Wooten [a], Elizabeth Asque [a], Min Hu [a], Carolin Hoft [b], Ryan Duggan [a], Matthew Townsend [c], Karin Orsi [d], Karen Dalecki [e], Willi Amberg [b], Lori Duggan [d], Heather Knight [d], Joseph S. Spina [d], Yupeng He [a], Kennan Marsh [a], Vivian Zhao [f], Suzanne Ybarra [f], Jennifer Mollon [g], Yuni Fang [f], Aparna Vasanthakumar [a], Susan Westmoreland [d], Mathias Droescher [b], Sjoerd J. Finnema [a], Hana Florian [a]

[a] *AbbVie Inc., North Chicago, IL, United States*
[b] *AbbVie Deutschland GmbH & Co. KG, Neuroscience Research, Knollstrasse, 67061, Ludwigshafen, Germany*
[c] *AbbVie, Cambridge Research Center, 200 Sidney Street, Cambridge, MA, 02139, United States*
[d] *AbbVie Bioresearch Center, 100 Research Drive, Worcester, MA, 01605, United States*
[e] *Former AbbVie Employee, United States*
[f] *AbbVie Bay Area, 1000 Gateway Boulevard, South San Francisco, CA, 94080, United States*
[g] *AbbVie Deutschland GmbH & Co. KG, Statistical Sciences and Analytics, Knollstrasse, 67061, Ludwigshafen, Germany*

A B S T R A C T

Alzheimer's disease (AD) is the most common global dementia and is universally fatal. Most late-stage AD disease-modifying therapies are intravenous and target amyloid beta (Aβ), with only modest effects on disease progression: there remains a high unmet need for convenient, safe, and effective therapeutics. Senescent cells (SC) and the senescence-associated secretory phenotype (SASP) drive AD pathology and increase with AD severity. Preclinical senolytic studies have shown improvements in neuroinflammation, tau, Aβ, and CNS damage; most were conducted in transgenic rodent models with uncertain human translational relevance. In this study, aged cynomolgus monkeys had significant elevation of biomarkers of senescence, SASP, and neurological damage. Intermittent treatment with the senolytic navitoclax induced modest reversible thrombocytopenia; no serious drug-related toxicity was noted. Navitoclax reduced several senescence and SASP biomarkers, with CSF concentrations sufficient for senolysis. Finally, navitoclax reduced TSPO-PET frontal cortex binding and showed trends of improvement in CSF biomarkers of neuroinflammation, neuronal damage, and synaptic dysfunction. Overall, navitoclax administration was safe and well tolerated in aged monkeys, inducing trends of biomarker changes relevant to human neurodegenerative disease.

1. Introduction

By 2050, over 100 million individuals worldwide are projected to be diagnosed with the common, progressive, fatal neurodegenerative disease known as Alzheimer's Disease (AD). AD-related cognitive decline has been primarily attributed to the accumulation of CNS misfolded proteins, particularly amyloid beta (Aβ) and tau. Levels of misfolded proteins have been linked to progressive cortical atrophy, especially in the medial temporal lobe, hippocampus, and entorhinal cortex. Over 3 billion dollars are spent annually on

* Corresponding author.
E-mail addresses: edward.greenberg@abbvie.com, efgreenberg@gmail.com (E.F. Greenberg), martin.j.voorbach@abbvie.com (M.J. Voorbach).

https://doi.org/10.1016/j.heliyon.2024.e36483
Received 26 June 2024; Received in revised form 1 August 2024; Accepted 16 August 2024
Available online 17 August 2024

research focusing on AD and related dementias (media@alz.org, 2020), with hundreds of drugs now in clinical trials, primarily focused on the removal of these misfolded proteins [1]. Disappointingly, the best late-stage AD therapeutics only have modest clinical benefit. Aducanumab was granted conditional FDA approval for mild AD, based largely on its removal of amyloid plaques, with only modest effect on slowing cognitive decline [2]. With further large confirmatory studies needed for full approval, Biogen ultimately elected to terminate the aducanumab program [3]. Lecanemab, an anti-amyloid antibody with high selectivity for protofibrils, demonstrated a 27 % reduction in clinical decline on the Clinical Dementia Rating scale Sum of Boxes (CDR-SB) after 18 months of treatment compared to placebo in a Ph3 study ([4], [5]). Donanemab, another advanced anti-amyloid AD therapeutic, which markedly lowers Aβ levels, similarly reduced cognitive decline by 30 % in a Phase 2 study (iADRS and ADAS-Cog decline at 76 weeks) [6].

The focus on misfolded protein removal may be a key factor in the limited clinical benefit seen with investigational AD therapeutics. While misfolded proteins can directly impair neuron viability in vitro and in preclinical models [7], the direct neurotoxicity of these aggregates may not be the primary driver of human disease. The accumulation of misfolded proteins with age does not inevitably result in cognitive decline: almost half of nonagenarians and almost all centenarians accumulate significant levels of CNS Aβ and tau, but many retain normal cognition throughout their lifetimes even with extraordinarily high misfolded protein levels [8]. At the same time, key features of AD CNS pathology often appear years before overt cognitive decline. The timing of typical AD interventions (i.e., at symptom onset) may be too late to make a meaningful difference in disease progression. Earlier interventions when cognitive symptoms are minimal may be more effective; to be practical, they would need to be simple, well-tolerated, and ideally fixed in duration.

An emerging theory is that significant AD-related neurodegeneration only occurs when misfolded proteins and/or other toxic insults trigger an exaggerated downstream neuropathological response. In addition to the accumulation of aggregated Aβ and tau, AD is also characterized by defects in proteostasis [9], lysosomal dysfunction [10], mitochondrial dysfunction [11], and increased neuroinflammation [12]. Dysfunctional proteostasis and lysosomal function interfere with Aβ and tau degradation [9] and clearance [10]; defective mitochondria increase reactive oxygen species (ROS) and ROS-induced protein misfolding; and neuroinflammation can accelerate the formation and transmission of protein aggregates throughout the CNS in a progressive downward spiral [13]. To make a meaningful difference in clinical progression, disease-modifying AD therapeutics may need to modulate additional downstream drivers of neurodegeneration beyond misfolded proteins.

A key mediator of the disparate pathological features of AD is the accumulation of senescent cells (SC). DNA damage can be induced by a wide variety of cellular stressors, including Aβ [14] and tau [15], ultimately inducing oncogenesis if left unchecked. To prevent tumor formation, many DNA-damaged cells often undergo apoptosis. However, some DNA-damaged cells override the normal apoptotic response by upregulating the expression of anti-apoptotic proteins, particularly the B-Cell lymphoma 2 (Bcl-2) family members Bcl-2 and Bcl-xL (AKA BCL2L1). These SC are still metabolically active, with a pro-inflammatory senescence-associated secretory phenotype (SASP).

Senescence and SASP contribute to multiple pathological features of neurological disorders, including proteostasis defects [16,17], neuroinflammation [18,19], dysfunctional mitochondria [20–22], and accumulation of misfolded proteins [18,19,23,24]. Therapeutics that selectively remove senescent cells, termed “senolytics,” may therefore reduce multiple drivers of neurodegeneration and have a more profound clinical effect than protein aggregate removal alone. In addition, SC take several weeks to reaccumulate once removed by virtue of their irreversible cell cycle arrest [25], suggesting senolytics may only need to be given intermittently in order to produce durable benefits.

The dependence of many SC on Bcl-2 family members for survival suggests an “Achilles heel” for therapeutic intervention. Dual knockdown of Bcl-2 and Bcl-xL has been demonstrated to selectively kill SC from a wide range of cell lineages, while sparing their nonsenescent counterparts [26,27]. Navitoclax, an orally bioavailable selective inhibitor of Bcl-2 and Bcl-xL, has been published to have potent preclinical senolytic activity across multiple tissue types [27,28]. In aged wild-type (WT) mice, navitoclax was shown to kill senescent CNS neural precursor cells, boost hippocampal neurogenesis, and improve spatial memory [29]. Similarly, treating PS19 tauopathy mice with intermittent cycles of navitoclax reduced levels of senescent glia, lowered hippocampal and cortical inflammatory markers, and decreased tau aggregate accumulation [19].

Studies of other senolytics in preclinical neurodegenerative disease models have also suggested disease-modifying effects. A recent study of dasatinib and quercetin (D + Q) in the APPPS1 amyloidopathy mouse model was shown to reduce the burden of senescent oligodendrocyte precursor cells (OPC), decrease amyloid beta, and improve cognition [30]. In a separate study, D + Q reduced neuroinflammation, lowered neurofibrillary tangles (NFT), and increased levels of neuronal proteins in aged rTg4510 Mapt-null tauopathy mice [23]. While encouraging, all the above studies have been performed on genetically limited rodent models, often relying on transgenic overexpression of specific amyloid or tau isoforms. As such, the translational relevance of these studies to human neurodegenerative disease is limited at best.

In contrast, cynomolgus non-human primates (NHP) have over 90 % DNA sequence identity to humans [31], and share >80 % of human brain prefrontal cortex gene expression [32]. Like humans, NHP accumulate SC across tissues with age [33,34], particularly in vascular, skin, and immune systems [35]. Aged NHP also naturally develop human-like neurodegenerative pathology, with evidence of age-related amyloid plaques, aggregated tau hyperphosphorylation, and other AD-like lesions [32,36].

In this series of studies, we first assessed pharmacokinetics and CNS penetration of navitoclax in rodents (wild type mice and rats). With the translational relevance of NHP in mind, we then performed a comparative study of aged vs young cynomolgus monkeys, showing significant age-dependent enrichment of SC and SASP markers in the skin, blood, and CSF. In a subsequent study of navitoclax in aged NHP, we demonstrated navitoclax blood-brain-barrier (BBB) penetration at senolytic-relevant concentrations; acceptable safety and tolerability; reductions in selected systemic and CNS SC and SASP; and modulation of AD-relevant CSF biomarkers.

2. Materials/methods

Rodent animals and drug treatment: Mice were treated under German federal authority approval (code A17-9-005). Rats were treated under Institutional Animal Care and Use Committee (IACUC) protocols (IACUC protocol number 0812A01245), in accordance with local regulatory authorities. C57BL/6JRj mice (WT mice) were purchased from Janvier labs. Male Rat-CD® rats (Sprague Dawley, IGS Rat Strain 001) were acquired from Charles River Laboratories, inc. All [^{14}C]navitoclax and navitoclax aliquots were produced by AbbVie, Inc. The single dose pharmacokinetics of [^{14}C]navitoclax (10 mg/kg, single dose, administered by oral gavage in 2 % DMSO/5 % Tween 80/20 % PG/73 % D5W) was evaluated in rats (n = 12). Multiple dose pharmacokinetics of navitoclax (50 mg/kg/day x five days, administered by oral gavage in 10 % EtOH/30 % PEG 400/60 % Phosal 50 PG) was evaluated in WT mice (n = 3) by determining the compound's plasma and brain concentration on the first and fifth day of dosing. Mice were perfused prior to brain harvesting to remove residual capillary blood from the tissues. Drug concentrations were determined by LC-MS/MS.

NHP animals and drug treatment: Animals were treated under IACUC protocols (IACUC protocol numbers 1808C00027 and 2108C00039) in accordance with local regulatory authorities. Two cohorts of young (4–8 years old at baseline) and aged (17–25 years old at baseline) cynomolgus monkeys (*Macaca fascicularis*) were included in the study. Only baseline blood for PBMCs (2 mL/NHP in EDTA tubes) and CSF (1 mL CSF/NHP) samples were collected from NHP in cohort 2, comprising 12 aged NHP (AA1-12) and 21 young NHP (YY1-21). Unless otherwise specified, all other NHP methods refer to cohort 1, comprising 6 aged NHP (A1-6) and 13 young NHP (Y1-13).

Senolytic intervention in NHP was performed with navitoclax administered as an amorphous solid dispersion (ASD). Navitoclax ASD was mixed in food and administered orally once a day at an initial "low-dose lead-in" of 1.44 mg/kg/day x five days of treatment, followed by 16 days of rest. Navitoclax "full dose" was then administered on a repeating regimen of 12 mg/kg/day x 5 days of treatment followed by 16 days of rest. Six complete cycles of full dose navitoclax ASD were administered. NHP were housed in a 12h:12h light:dark cycle environment in pathogen-free barrier conditions. Compliance with relevant ethical regulations and all animal procedures were reviewed and approved by the IACUC (IACUC protocol numbers 1808C00027 and 2108C00039). Baseline blood (19–21 mL/NHP, divided between PAXgene blood RNA tubes and EDTA tubes), skin (three 4–6 mm skin punch biopsies/NHP: one formalin-fixed paraffin-embedded, one placed in RNAlater, one flash frozen), and CSF (1 mL CSF/NHP) samples were collected from all NHP in cohort 1, comprising six aged NHP (2 samples for A6, 1 sample for all other aged NHP) and 13 young NHP (1 sample/NHP). Blood (14 mL/NHP) and skin samples (three 4–6 mm punch biopsies) were also collected at Day 7 and Day 21 of each navitoclax cycle. Post-navitoclax CSF samples for biomarkers of neuroinflammation and neuronal damage were collected from four aged NHP (A1, A2, A3, and A4). Navitoclax CSF samples (0.5–1 mL CSF/NHP) were collected from four aged NHP (A2, A4, A5, and A6) 24 h after completing daily doses with navitoclax (12 mg/kg/day x 5 days, ASD mixed in food). A ~10–50 μL volume of CSF was used for each CSF PK analysis; the remainder was used for CSF biomarker analysis.

NHP plasma and hematology analyses: Multiple dose pharmacokinetics and hematology were evaluated in two chair-trained aged NHP (A1 and A2) on Days 1–5 of daily navitoclax dosing. Hematology samples were also collected from four aged NHP (A1, A2, A3, and A4) on Day 7 of each navitoclax cycle. K_2EDTA blood samples were obtained from a femoral artery or vein of each animal 24 h after compound administration from Days 1–5. Samples were profiled on a Cell Dyne 3700 hematology analyzer according to the manufacturer's recommendations. Plasma was separated by centrifugation (~4 °C) and navitoclax separated using protein precipitation with acetonitrile containing the stable label internal standard (SLIS). A 10–50 μL plasma aliquot was used for each plasma PK analysis, further described in "NHP PK analyses" below; the remainder was used for plasma biomarker analysis.

NHP PK analyses (plasma and CSF): For both plasma and CSF PK analyses, navitoclax and the SLIS were separated from each other and co-extracted contaminants on a 30 × 2.1 mm Waters X-Bridge C18 5 μm column with an acetonitrile in 0.2 %/1 mM aqueous ammonium hydroxide gradient mobile phase at a flow rate of 1.5 mL/min. Analysis was performed on a Sciex API6500+™ Biomolecular Mass Analyzer with a turbo ionspray interface. Navitoclax and internal standard peak areas were determined using Sciex Analytst™ software. The plasma drug concentration of each sample was calculated by least squares linear regression analysis (non-

Table 1
NHP CSF biomarkers.

Biomarker	CSF dilution	Method
tTau	1:10	SMC
pTau199	1:6	SMC
pTau231	1:8	SMC
pTau396	1:6	SMC
Vilip 1	1:8	SMC
Nf-L	1:40	SIMOA
Gap43	1:20	Ella
MCP-1	1:20	Ella
sTREM2	1:20	Ella
YKL-40	1:20	Ella
Amyloid Aβ 1-38	1:10	MSD
Amyloid Aβ 1-40	1:10	MSD
Amyloid Aβ 1-42	1:10	MSD

Abbreviations: SMC, Single Molecule Counting; Ella, Ella automated immunoassay; MSD, Meso Scale Discovery. SIMOA, Single Molecule Array.

weighted) of the peak area ratio (parent/internal standard) of the spiked plasma standards versus concentration.

NHP plasma biomarker analyses (protein levels): NHP platelet-poor plasma (0.5 mL/NHP) was diluted 1:2 to 1:8 to ensure assay linearity, then profiled for protein levels of interest via the following ligand-binding assays: 1) MILLIPLEX MAP Non-Human Primate Cytokine Magnetic Bead Panel (PCYTMG-40K-PX23); Millipore Human MMP Magnetic Bead Panel 2 - (HMMP2MAG-55K); IBL HMGB1 ELISA (Tecan ST51011); Human u-PAR Quantikine ELISA Kit (R&D DUP00).

NHP CSF biomarker analysis (protein levels): Baseline CSF Nf-L analyses were performed on all available NHP CSF samples (n = 13 young, n = 5 aged: A1, A2, A3, A4, and A6). For A4 and A6, two separate baseline CSF samples were collected; for all other aged NHP, one baseline CSF sample was collected. Post-navitoclax CSF Nf-L analyses were performed on four aged NHP (A1, A2, A3, and A4). Due to international regulatory and operational complications, all other post-navitoclax CSF protein level analyses were only performed on samples from two aged NHP (A2 and A4). CSF (10–50 μL/assay) was diluted 1:8 to 1:20 to ensure assay linearity, then profiled for protein levels of interest via Merck Millipore Single Molecule Counting technology (SMC), Proteinsimple Simpleplex Ella (Ella), Meso Scale Discovery (MSD), and Quanterix SIMOA HD-X (SIMOA) platforms. Further details of CSF biomarkers analyzed are provided in Table 1.

NHP skin histology: NHP epidermal skin samples (4–6 mm back punch biopsies, yielding ~10 mg tissue) were fixed in 10 % NBF, processed and paraffin-embedded routinely, and microtome sectioned at 5 μm. Immunohistochemistry was run on a Leica Bond RX (Leica Biosystems, Deer Park, IL), with minor modifications from that described previously [37,38]. Primary antibodies used: rabbit anti-human lamin B1, Abcam ab16048 [1 μg/ml]; rabbit mAb anti-human HMGB1, Cell Signaling 6893 [2.5 μg/ml]; both were detected with Leica's goat anti-rabbit/HRP polymer, visualized with chromogen DAB (3,3-Diaminobenzidine) and counterstained with hematoxylin. Imaging was performed using a 3DHISTECH scanner. VisioPharm software was used for automated image acquisition and analysis. The number of positive cells for a given marker were standardized to the total number of nuclei present in each section.

Quantitative RT-PCR (RT-qPCR): Analyses were performed on NHP skin, whole blood, and PBMCs. NHP skin punch biopsies: 4–6 mm skin punch biopsies were collected and treated with RNAlater according to manufacturer's protocol, (AM7021, Invitrogen). Each biopsy was cut in half and homogenized in a 2 mL Eppendorf Safelock tube with 700 μL Qiazol (79306, Qiagen) and Garnet PowerBead Tubes 0.7 mm (13123-50, Qiagen). Tissue lysates were incubated at room temperature for 5 min. Chloroform, 140 μL, (C2432, Millipore Sigma) was added to each sample, then vortexed on high speed for 15 s. Samples were allowed to incubate at room temperature for 2 min. Organic phase separation was carried out at 4 °C 12,000×*g* for 15 min 350 μL of the resulting aqueous layer was transferred to a 2 mL Eppendorf Safelock microcentrifuge tube and processed through the miRNeasy mini kit via the Total RNA isolation protocol (217004, Qiagen) according to manufacturer's protocol on the Qiacube Classic (9001292, Qiagen). NHP whole blood: 2.5 mL was collected into a PAXgene Blood RNA tube and prepared following manufacturer's protocols (762165, PreAnalytix/Qiagen). Total RNA from NHP whole blood was isolated on the QIAsymhpony (9001297, Qiagen) with the QIAsymphony PAXgene Blood RNA kit (762635, Qiagen) following manufacturer's protocol with UltraPure water (10977023, Invitrogen) used as the elution buffer. NHP PBMCs: PBMCs were isolated from 4 mL of NHP whole blood within 8 h post blood draw. Total RNA from PBMCs was isolated using organic phase extraction and the miRNeasy micro kit (217084, Qiagen) on the Qiacube Classic (9001292, Qiagen) following manufacturer's protocol. RT-QPCR: Total RNA from skin, whole blood, and PBMC was converted to cDNA with SuperScript IV VILO (11756050, Invitrogen). Specific Target Amplification was performed following manufacturer's protocol (Fluidigm ref 68000133 D2) with the following gene targets: p16, p21, IL-6 and TNFα were as previously described [25], IL-1β, IL-8 and MCP-1 were as previously described [39,40], ACTB forward 5′- CACCATTGGCAATGAGCGGTTC -3′, reverse 5′- AGGTCTTTGCGGATGTCCACGT-3′. 14 PCR cycles were used for pre-amplification of all samples, post pre-amplification all samples were diluted 1:5 with DNA Suspension buffer, pH 8.0 (T0223, Teknova). Samples were loaded on the Fluidigm 192.24 IFC dynamic array (100.6265, Fluidigm) following manufacturer's protocol for the Juno and RT-qPCR data capture was performed on the BioMark HD (Juno, BMKHD, Fluidigm). Expression for all experiments was normalized first to ACTB.

TSPO-PET: NHP imaging was performed at baseline and at the completion of all navitoclax treatment (228 ± 60 days apart). Briefly, animals were fasted for 18–24 h prior to PET and anesthetized using isoflurane (2–2.5 %) throughout the scan. After animal anesthesia and preparation, a CT of the brain was acquired using a Ceretom system (Neurologica, Danvers, MA) for use in PET attenuation correction. Dynamic [^{18}F]PBR111 [41] PET data 120 min in duration were collected in aged (n = 6) male (n = 4) and female (n = 2) cynomolgus NHP (6.0 ± 1.1 kg) on a Focus220 system (Siemens, Knoxville TN). Arterial blood samples were collected for measurement of the arterial input function of the PET tracer. In one PET measurement arterial blood sampling was not successful. Body temperature was maintained at 37 °C using a heated water blanket and hot air. Vital signs were monitored throughout the scanning procedure. The injected amount of radioactivity was 4.92 ± 1.66 mCi, molar activity was 2846 ± 1708 Ci/mmol, and mass amount was 0.85 ± 0.35 μg. For image analysis, subject-space MRI and neuroanatomical atlas were coregistered to PET images of each animal to derive regional time activity curves. Total volume of distribution ratio (DVR) was computed using the Logan graphical method with the cerebral white matter as reference region [42].

Apoptotic Body Flow Cytometry (FCM): NHP whole blood samples were separated into intact cells (WBCs) and platelet poor plasma (PPP) by centrifugation as described previously [43]. PPP and WBC were incubated separately with an apoptosis dye (ApoTracker Green, BioLegend #427402), then further incubated with antibodies against the following cell surface epitopes: WBC subtype markers (mouse anti-human CD3-BUV395 for T cells, BD Biosciences clone SP34; mouse anti-human CD14-BUV805 for monocytes, BD biosciences clone M5E2; mouse anti-human CD20-BV711 for B cells, BioLegend clone 2H7; mouse anti-human CD56-PE for NK cells, BioLegend clone 5.1H11) and senescence-enriched markers (anti-B2M-PECy7, clone 2M2, BioLegend; anti-CD26-PerCP-Cy5.5 BioLegend clone BA5b, mouse anti-CCR6-BV421 AKA CD196, BioLegend 353408; APC mouse anti-DEP1, Abcam ab234278; purified anti-CD87 AKA uPAR, ThermoFisher, MA5-38490 – custom conjugated to CF680 using the Mix-n-stain protein labeling kit from Biotium). All antibodies were used at the recommended 5 μL test size in a final staining volume of 100 μL (1:20 dilution). Flow

cytometry methods were performed as previously described [44]. Briefly, samples were analyzed using the Aurora Spectral Analyzer (Cytek Biosciences) with log forward scatter (FSC) and side scatter (SSC) detection to ensure proper resolution of the small apoptotic bodies. FSC and SSC resolution of small particle detection in the range of 0.5–2 μm in size was calibrated using the Nano Blank Polystyrene size standard kit – 0.1 μm–2.0 μm (Spherotech, Inc.) – *data not shown*. Instrument fluorescent ranges (−13000 to 4194304) were rescaled via analysis software to a range of −4 to 10. Negative values represented spreading error post spectral deconvolution and were interpreted as lacking expression of a given marker. Values 1–2 were no/minimally expressed markers; values 2–4 were moderately expressed markers; values > 4 were highly expressed markers. A gating strategy was used to maximize the purity of each immune cell subtype, identify it as apoptotic, and assess the expression of the senescence markers. Briefly, populations were gated by size via FSC-A and SSC-A to enrich for intact particles in the size range of the calibration beads (~1 μm), then further gated on ApoTracker green positivity indicating an event as an Apoptotic Body, followed by a positive signal of the desired lineage marker (e.g., $CD3^+$ or $CD14^+$), and finally for the presence or absence of one of the senescence markers. Proportions of cells with a given cell surface senescence marker were reported as a percentage of total Apoptotic Bodies present in the sample.

Statistical analysis: Plots of CSF biomarkers, PK data, and PBMC cell surface markers were generated using R for Windows V4.1.2 [45] and R package ggplot2 V3.3.6 [46]. All other plotting and data analysis was done in GraphPad Prism version 9.1.0 for Windows, GraphPad Software, San Diego, California USA, www.graphpad.com. HMGB1 and lamin B1 epidermal expression were compared between groups using an unpaired *t*-test. A mixed model was fitted to the repeated measures in transcription profiles in skin and blood and each post-treatment time point was tested for significant difference compared to baseline. Group comparisons of transcription profiles in blood were tested using Welch's test, or in the presence of large outliers (IL-6, MCP-1), using a Mann-Whitney test. Group comparisons of protein biomarker profiles in plasma and CSF were tested using a Mann-Whitney test. A paired *t*-test was performed for each TSPO-PET brain region. All p-values were uncorrected unless otherwise stated. The following denotes significance in all figures: $*P < 0.05$, $**P < 0.01$, $***P < 0.001$. Box-and-whisker plots denote the lower quartile, median, and upper quartile, with whiskers extending to the minimum and maximum values. Plots with error bars denote the mean ± 1 SEM. Given the small number of animals and the exploratory nature of this study, no power calculations were used. A5 and A6 samples were excluded from post-navitoclax assessments of senescence, SASP, and neuronal damage, given navitoclax dosing irregularities and elapsed time (>12 months) between baseline samples and navitoclax administration.

3. Results

3.1. Navitoclax CNS penetration in rodents

Though senolytic activity of navitoclax across tissue types has been widely reported [19,27,28,47,48], it has been uncertain if navitoclax has sufficient.

BBB permeability to have direct CNS effects. To assess the CNS penetration of navitoclax, we administered navitoclax (50 mg/kg/day x 5 days) to C57BL/6 mice, achieving a total brain concentration of 42 nM at the terminal timepoint 24h after the last dose (Fig. 1a). [^{14}C]Navitoclax (10 mg/kg/day x 1 day) was also administered to male rats, resulting in a peak total brain concentration (navitoclax and metabolites) of 42 nM, with a 2–3% brain/plasma ratio (Fig. 1b).

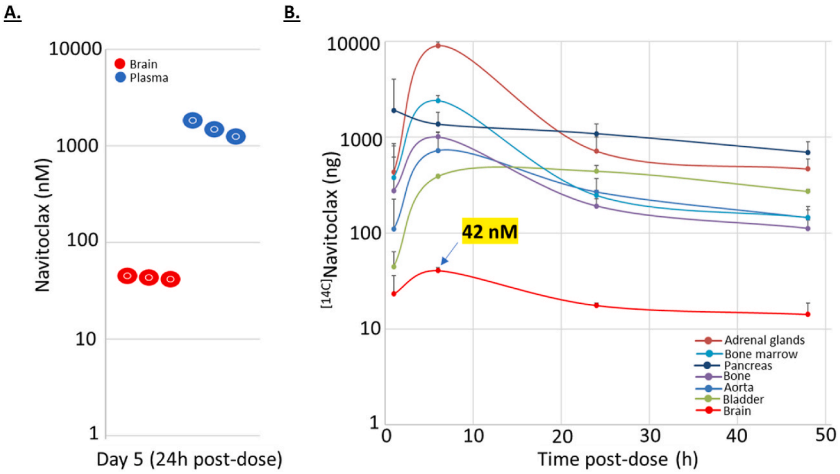

Fig. 1. Navitoclax reaches senolytic-relevant concentrations in the rodent CNS.
A. Navitoclax (**50 mg/kg/day x 5 days**) was administered to C57BL/6 mice (n = 3). Navitoclax concentrations in the brain and plasma were assessed 24 h following the last dose of navitoclax. **B.** [^{14}C]Navitoclax (**10 mg/kg/day x 1 day***)* was administered to male rats. Tissue concentrations of radioactivity were then assessed at 1–120 h following navitoclax administration.

3.2. Intermittent navitoclax in aged cynomolgus monkeys

We next aimed to validate the role of senescence and navitoclax activity in aged cynomolgus macaques, an animal model with more human translational relevance than rodent models (Fig. 2, Table 2). Briefly, baseline blood, skin, and CSF samples (senescence, SASP, neurodegeneration, Aβ) were collected from young (age 4–7 YO) and aged (age 17–23 YO) cynomolgus monkeys. Baseline imaging assessments (TSPO-PET) were also collected from aged (age 17–23 YO) cynomolgus monkeys. Aged NHP (n = 6) were then treated with one three-week cycle of low-dose oral navitoclax (**1.44 mg/kg/day x 5 days**), followed by six cycles of full-dose navitoclax (**12 mg/kg/day x 5 days/cycle**), based on published navitoclax treatment in PS19 tauopathy mice [19]. Skin and blood assessments were repeated each cycle, while CSF and imaging studies were repeated after completion of navitoclax treatment.

Due to operational challenges, A5 and A6 navitoclax dosing began >1 year after baseline blood, skin, and CSF samples were collected; these animals were excluded from post-navitoclax analyses for these biomarkers. On analysis, many plasma proteins were below the lower limit of quantitation. Plasma protein levels did not show significant differences between baseline aged and young NHP, nor were pre- and post-navitoclax treatment differences appreciated (*data not shown*), and these studies are not further discussed.

CSF samples were originally planned to be collected 24 h following the last dose of navitoclax in cycle 6. Due to technical challenges, only 2/4 of the original navitoclax-treated aged NHP had successful post-navitoclax CSF collections. An additional two aged NHP (A5 and A6) were subsequently treated with navitoclax, with CSF collected 24 h post-navitoclax. Baseline PBMC and CSF samples were also collected from a second cohort of 12 aged NHP (AA1-12) and 21 young NHP (YY1-21). Details of NHP demographics are provided in Supplementary Table 1 (cohort 1) and Supplementary Table 2 (cohort 2).

3.3. Navitoclax safety/tolerability, PK, and effects on peripheral SASP

Overall, navitoclax treatment was safe and well-tolerated in aged NHP. Consistent with its mechanism of action, navitoclax induced moderate thrombocytopenia in all animals; this was not associated with significant bleeding, and platelet counts rapidly returned to baseline upon withdrawal of study drug (Fig. 3a). Navitoclax was detectable in the CSF of aged NHP 24 h after study drug administration, with a peak detectable concentration of 1.7 nM (median 0.30 nM, mean 0.56 nM), and CSF:plasma ratios ranging from 0.03 to 0.9 % (Fig. 3b).

NHP whole-blood samples showed marked age-dependent increases in mRNA markers of senescence, including a 2.7-fold increase in p16 mRNA and a 2-fold increase in IL-8 mRNA (Fig. 3c, top). Similar age-dependent elevation was also seen in blood SASP mRNA markers MCP-1 and IL-1b. Navitoclax treatment induced reductions of whole-blood RNA senescence (p16) and SASP (IL-8, MCP-1, IL-1b, and IL-6) in two of the four aged NHP, with peak effects appreciated by cycle 3. The remaining two aged NHP did not show significant post-navitoclax blood biomarkers (Fig. 3c, bottom).

To confirm and expand on the trends noted in the whole-blood senescence and SASP RNA, PBMC samples were collected from a second cohort consisting of 12 aged NHP (AA1-12) and 21 young NHP (YY1-21). As with the whole-blood samples, PBMC samples showed significant age-dependent increases in mRNA markers of senescence, including a 1.6-fold increase in p16 mRNA, a 1.3-fold increase in p21 mRNA and a 3.1-fold increase in IL-1β mRNA (Fig. 3d). Similar trends in age-dependent elevation were also seen in SASP mRNA markers TNFa and MCP-1.

To further investigate the effect of navitoclax on circulating senescent cells, blood samples were enriched for PBMCs, sorted via fluorescence-activated cell sorting (FACS), and profiled for cell surface markers of senescence. Navitoclax treatment was associated with a decline in CD20+β2M + B lymphocytes as a percentage of total cells (5-10x vs baseline), with post-treatment effects observed in all four aged NHP. Peak effect was observed by cycle 4, and levels remained suppressed 16 days post-treatment (Fig. 3e, top left). Navitoclax induced a similar trend of reduction in $CD14^{+}$ β2M + monocytes (Fig. 3e, bottom left), CD3+β2M + T lymphocytes (Fig. 3d, top right), and CD56+β2M + NK cells (Fig. 3e, bottom right) in the four aged NHP. CD26, CCR6, uPAR, and DEP1 levels did not show

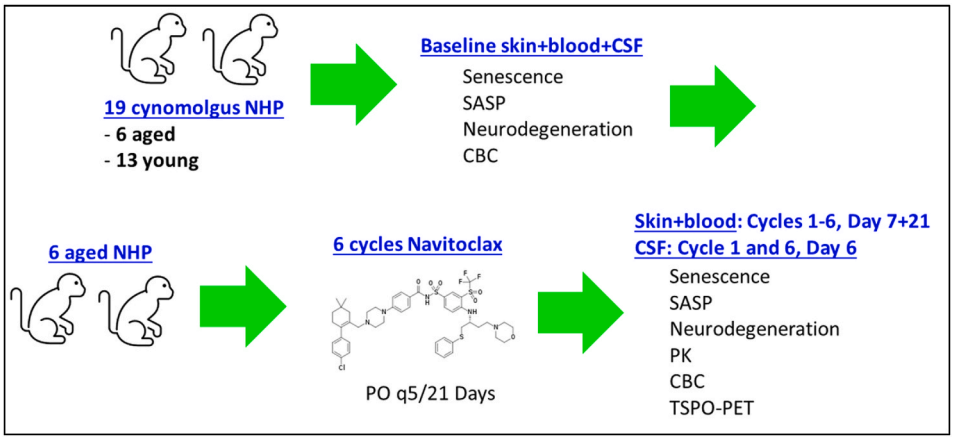

Fig. 2. Navitoclax in NHP study schema.

Table 2
Navitoclax in NHP study activity schedule.

Activity	Baseline	Lead-in[a],[e], Cycles 1–6[b],[e]							EOT[d]
		D1	D2	D3	D4	D5	D6	D8	
Physical Examination	X	X	X	X	X	X	X	X	
Blood for Hematology (CBC)	X	X	X	X	X	X	X	X	
Blood for Clinical Chemistry	X	X	X	X	X	X	X	X	
Skin for biomarkers (senescence, SASP)	X	X							
CSF for biomarkers (SASP, neurodegeneration, Aβ)	X						X[c]		X
Blood for biomarkers (senescence, SASP, apoptotic bodies, neurodegeneration, Aβ)	X	X							
CSF for navitoclax PK[e]							X[c]		
Blood for navitoclax PK[e]			X	X	X	X	X		
Navitoclax treatment[e]		X	X	X	X	X			
TSPO-PET[e]	X								X

[a] Navitoclax lead-in dosing: 1.44 mg/kg x 5/21 days.
[b] Navitoclax Cycles 1–6 (C1-6) dosing: 12 mg/kg x 5 days/cycle, 21 days/cycle.
[c] Post-baseline CSF samples were collected on cycle 1 only.
[d] EOT: End of Treatment visit, approximately 30 days after the last dose of navitoclax.
[e] Aged NHP only.

significant modulation with navitoclax treatment (*not shown*). Similarly, NHP skin samples also showed marked age-dependent increases in several senescence markers, with a 2-fold elevation of bulk skin p21 mRNA, and a 25–35 % reduction in nuclear lamin B1 and HMGB1 in non-cornified epidermal cells (Fig. 3f). Navitoclax treatment partially reversed these skin senescence markers in all four aged NHP, with responses observed as early as cycle 3 (Fig. 3f).

3.4. Navitoclax effects on imaging and CSF biomarkers of SASP and neurodegeneration

NHP CSF and plasma samples were assessed by ligand binding assays for age-related and navitoclax-induced changes in AD-relevant soluble protein biomarkers. Several CSF biomarkers with significant age-dependent differences were identified at baseline levels, including MCP-1 (2.75-fold increase); YKL-40 (1.43-fold increase); Gap43 (2.01-fold decrease); neurofilament light (Nf-L, 1.84-fold increase); and sTREM2 (1.96-fold increase). (Fig. 4a–d, left). An independent comparison of a second cohort of young (N = 21) vs aged (N = 12) confirmed age-dependent changes in protein biomarkers (Fig. 4e–f). Post-navitoclax CSF samples obtained from two aged NHP showed trends of partial reversal of many age-dependent changes, inducing a 3.68-fold decline in MCP-1, a 1.7-fold decline in YKL-40, a 2.38-fold increase in Gap43, and a 1.63-fold reduction in NF-L (Fig. 4a–d, right).

Finally, TSPO-PET was performed in all aged NHP before and after navitoclax treatment. Frontal cortex TSPO-PET showed a significant reduction following navitoclax treatment; no other brain regions showed significant pre- and post-navitoclax treatment differences (Fig. 5).

4. Discussion

In this study, we have identified age-dependent changes in markers of senescence and SASP in the skin, blood, and CSF of aged NHP. Intermittent oral navitoclax administration was feasible, safe, and well-tolerated, with no serious treatment-emergent adverse effects. Intermittent navitoclax was associated with reduction in several systemic markers of senescence and SASP and achieved CSF concentrations at levels that may be relevant for senolytic activity based on previous preclinical studies. Finally, navitoclax treatment showed trends of improvement in CSF biomarkers of neuroinflammation (MCP-1, YKL-40), neuronal damage (NF-L), and synaptic integrity (GAP-43), along with an imaging biomarker of neuroinflammation (frontal cortex TSPO-PET).

This study provides uniquely detailed characterization of naturally occurring age-related NHP senescence and is one of the first long-term studies of a senolytic intervention in this animal model. Levels of senescent PBMCs increase significantly in human neurodegenerative disease, particularly senescent lymphocytes [49,50], and lymphocyte infiltration has been reported in the brains of patients with advanced human neurodegenerative disease [49,51–53]. The reduction in PBMC senescence markers in this study suggests an additional MOA for navitoclax CNS disease-modification.

While senescent β2M + cells have been reported to significantly increase in aged humans [54] and aged rodent brains [55,56], the use of this marker for assessing senescent PBMCs has not been widely established. Our study did also include more widely accepted markers of PBMC senescence, including p16, p21, and SASP markers (e.g., IL-1b), correlating with the β2M trends reported; nonetheless, further studies are warranted to further validate a link between β2M levels and PBMC senescence. Of note, β2M-directed therapies have been reported to selectively eliminate senescent cells [55,57], lower alpha-synuclein levels, and improve motor function in a rodent PD model [57]. The trends of navitoclax-induced reduction of β2M + cells across PBMC lineages suggests navitoclax may cause a similar reduction in β2M + senescent cells in the CNS.

Results from our study are consistent with prior navitoclax and ABT-737 studies in rodents, wherein treatment reduced systemic senescence and SASP [27,28,58,59], decreased markers of neuroinflammation and CNS senescence [19,29,58–60], lowered phosphorylated tau [19], and increased neurogenesis and cognitive performance [29,58]. Our results were also consistent with those

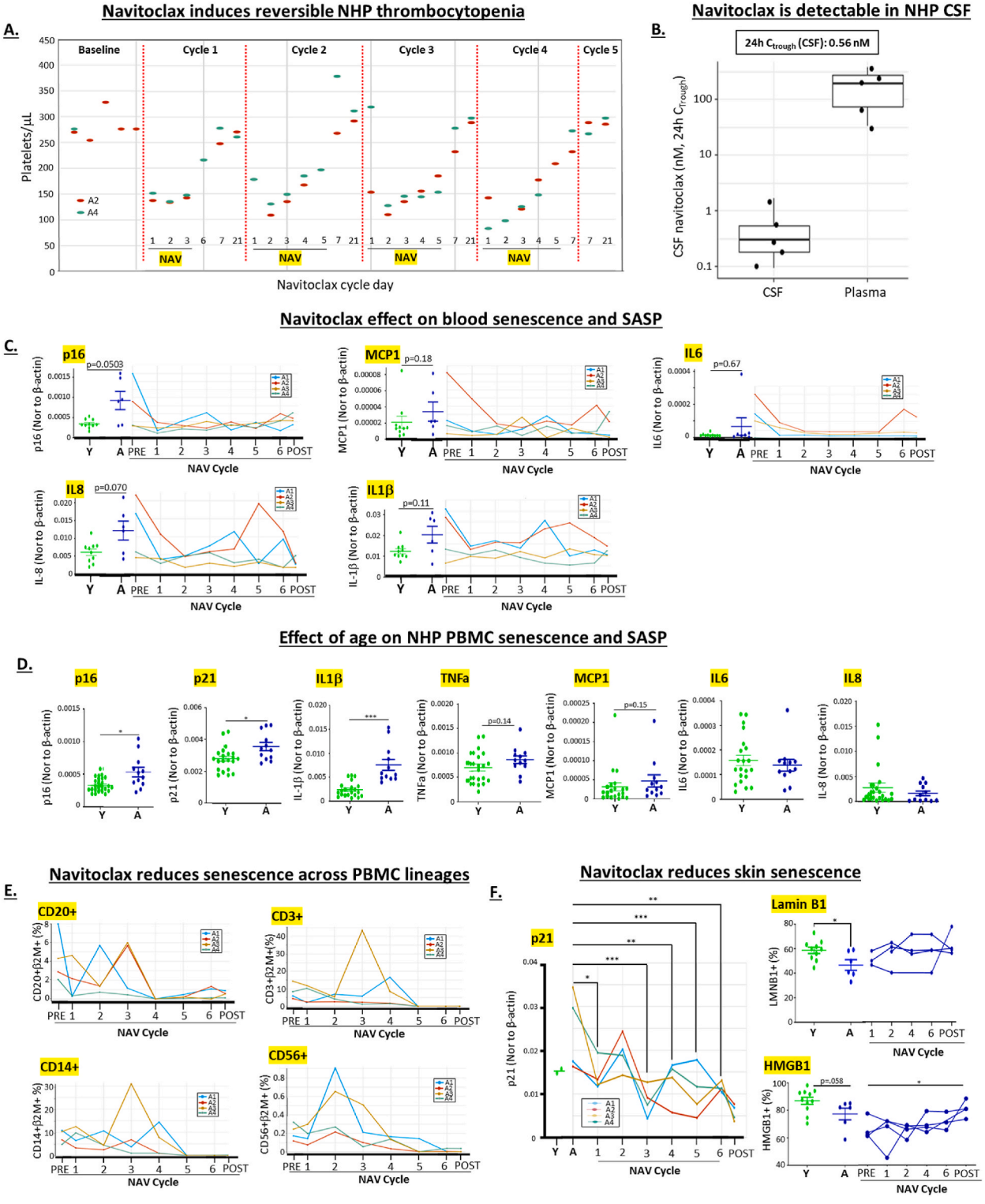

(caption on next page)

Fig. 3. Navitoclax has on-target thrombocytopenia, BBB penetration, and senolysis in aged NHP.
A. Effect of navitoclax on aged NHP platelet levels. Drug was administered Days 1–5 of each cycle. Shown: 2 aged NHP (A2, A4). **B**. Average 24h post-navitoclax CSF and plasma concentrations from aged NHP (A1, A2, A5 x 2, A6). Left: 24h CSF navitoclax = 0.56 ± 0.29 nM. Right: 24h plasma navitoclax = 190 ± 64 nM. **C.** Effect of age and navitoclax on mRNA markers of whole-blood senescence (p16) and SASP (IL-8, MCP-1, IL-1β, IL-6). *Left*: Baseline bulk blood mRNA. *Right*: Navitoclax effect**. D.** Effect of age on mRNA markers of PBMC senescence (p16, p21) and SASP (IL1b, TNFa, MCP1, IL6, IL8) in a second cohort of young (N = 21) and aged (N = 12). Statistical comparisons performed using Welch's *t*-test (p16, p21, IL1b, TNFa) or Mann-Whitney test (MCP1, IL6, IL8). **E.** Effect of navitoclax on cell surface senescence marker β2M+ in circulating PBMC. *Top left:* $CD20^+$ B lymphocytes/*Bottom left:* $CD14^+$ monocytes. *Top Right:* $CD3^+$ T lymphocytes. *Bottom right:* $CD56^+$ NK cells. PRE: Baseline, samples collected after 1 cycle of low dose navitoclax lead-in (1.44 mg/kg). POST: post-navitoclax, samples collected 16 days after the last dose of navitoclax cycle 6. **F.** Effect of age and navitoclax on markers of NHP skin senescence. *Left:* Effect of age and navitoclax on NHP bulk skin p21 mRNA. *Top right*: Effect of age and navitoclax on epidermal LMNB1 skin IHC. Results presented as % positive cells for LMNB1 vs total # non-cornified epidermal cells present. *Bottom right*: Effect of age and navitoclax on epidermal HMGB1. Results presented as % positive cells for HMGB1 vs total # non-cornified epidermal cells present. All PBMC and whole blood mRNA results presented as ΔΔCt = ΔCt (gene of interest mRNA)/−ΔCt (β-actin mRNA). Error bars: ±1 SE. *$p < 0.05$, **$p < 0.01$, ***$p < 0.001$. Abbreviations: NAV, navitoclax; β2M, beta-2 microglobulin. IHC, Immunohistochemistry; SC, senescent cells; SASP, Senescence Associated Secretory Phenotype; b-actin, beta-actin; SE, standard error; LMNB1, lamin B1; HMGB1, High mobility group box protein 1.

reported with the senolytic combination dasatinib and quercetin (DQ) in obese insulin-dependent NHP, wherein DQ reduced the burden of adipose SC, reduced markers of systemic SASP, and improved biomarkers of kidney function and metabolic parameters such as fasting glucose, hemoglobin A1c, total cholesterol, triglycerides, and kidney function [61,62]. In both the rodent and NHP studies, time-limited senolytic interventions produced significant improvements in disease-relevant biomarkers, supporting the applicability of senolytics to serious human disorders.

The administered aged NHP dose (12 mg/kg/day) is the human equivalent dose of approximately 270 mg, within the therapeutic range of 200–300 mg daily used in human oncology trials [63]. At this dosage, navitoclax was detectable in aged NHP CSF following oral dosing, supporting the potential of navitoclax for CNS disease-modification. While the absolute navitoclax CSF concentrations (0.09–1.7 nM) were low, they were within the range of levels needed to inhibit its Bcl-2 family targets [64] and induce cellular senolysis [27]. Moreover, navitoclax reaches its plasma C_{max} at 4–6 h following oral administration in dogs, with a half-life in cynomolgus monkeys of only 4–5 h [64]. As such, the 24h post-navitoclax CSF concentrations could significantly underrepresent the navitoclax CSF C_{max}.

Prior reports have shown limited BBB penetration of navitoclax in preclinical models [58,65,66]. It cannot be ruled out that navitoclax detectability in aged NHP CSF in our study could be a consequence of age-related increased BBB permeability in these animals [67]. Navitoclax has also been shown in prior animal studies to have effects on cerebral vasculature, with improvements in cognitive health linked to a combination of improved cerebral blood flow and modulation of peripheral inflammation [58,68]. As such, the observed impact of navitoclax on CSF biomarkers of SASP and neurodegeneration in this study may be attributable to its effects on peripheral senescent cells and cerebral vasculature, rather than direct effects on CNS senescent cells.

The study had a number of limitations. Only a small number of aged monkeys were available for this study, limiting its statistical significance and generalizability. In particular, post-navitoclax peripheral and CSF biomarkers could only be evaluated from four aged NHP. The effect of navitoclax on PBMC SASP was not assessed due to resource limitations and technical challenges. Future studies with larger sample size of aged monkeys are needed to confirm the post-navitoclax trends observed in whole blood senescence and SASP.

Our aged NHP also did not show classical AD biomarker enrichment (e.g., no significant changes in CSF tau, pTau, or Aβ with age), reducing the direct applicability of results to human AD. However, non-AD human neurodegenerative disorders such as Parkinson's disease (PD), amyotrophic lateral sclerosis (ALS), and multiple sclerosis (MS) share key pathological senescence-modulated features, including misfolded protein accumulation [69–72], dysfunctional proteostasis [73], and neuroinflammation [74–76]. Indeed, senescence has been directly linked to the pathophysiology of PD [37,77], MS [78,79], and ALS [80,81], and senomodulators have shown DMT effects in preclinical PD models [82]. NF-L has also become increasingly recognized as a predictive and prognostic biomarker across human neurodegenerative diseases [83]. The NF-L modulation seen with navitoclax in our study suggests it could have broad disease-modifying potential in CNS disorders. In order to assess the generalizability of the effects and navitoclax trends to human AD, further studies would be needed with animal models displaying classic AD pathological features.

TSPO-PET is a useful measure of neuroinflammation in neurodegenerative diseases [84]. Navitoclax treatment induced a significant reduction in TSPO DVR in the frontal cortex, although no significant effect was observed beyond this region. In NHP, TSPO PET signal across brain regions has previously been shown to decrease following microglia depletion with the CSF1R inhibitor PLX3397 and to increase following acute lipopolysaccharide administration in young NHP [85,86]. In aged NHP, TSPO-PET signal was found relatively high in striatal regions, hippocampus, temporal cortex, and thalamus, and positively correlated with amyloid-beta tracer [^{11}C]PIB binding in cortical regions [87]. Further evaluation of the regional effect of navitoclax on TSPO-PET is warranted.

Senolytics could potentially offer several advantages over existing AD therapeutics. While conventional therapeutics require daily dosing for continued efficacy, in preclinical studies senolytic effects persist for weeks following discontinuation of treatment [25]. Moreover, even partial SC removal appears sufficient for significant benefits, with a 30 % reduction in SC burden linked to meaningful improvements in preclinical pathology and function [25,88]. In contrast, in clinical studies, anti-amyloid therapeutics can achieve near-complete removal of amyloid plaques with only a 20–30 % reduction in cognitive decline at weeks 76–78 [2,6]. The durable benefits with short intermittent senolytic treatments may facilitate interventions at a presymptomatic phase, particularly with orally bioavailable therapeutics like navitoclax. Indeed, senolytics have now been safely administered in multiple clinical trials, with two senolytic studies now actively recruiting in AD: STOMP-AD [89] and ALSENlite NCT04785300. Our findings of navitoclax safety and

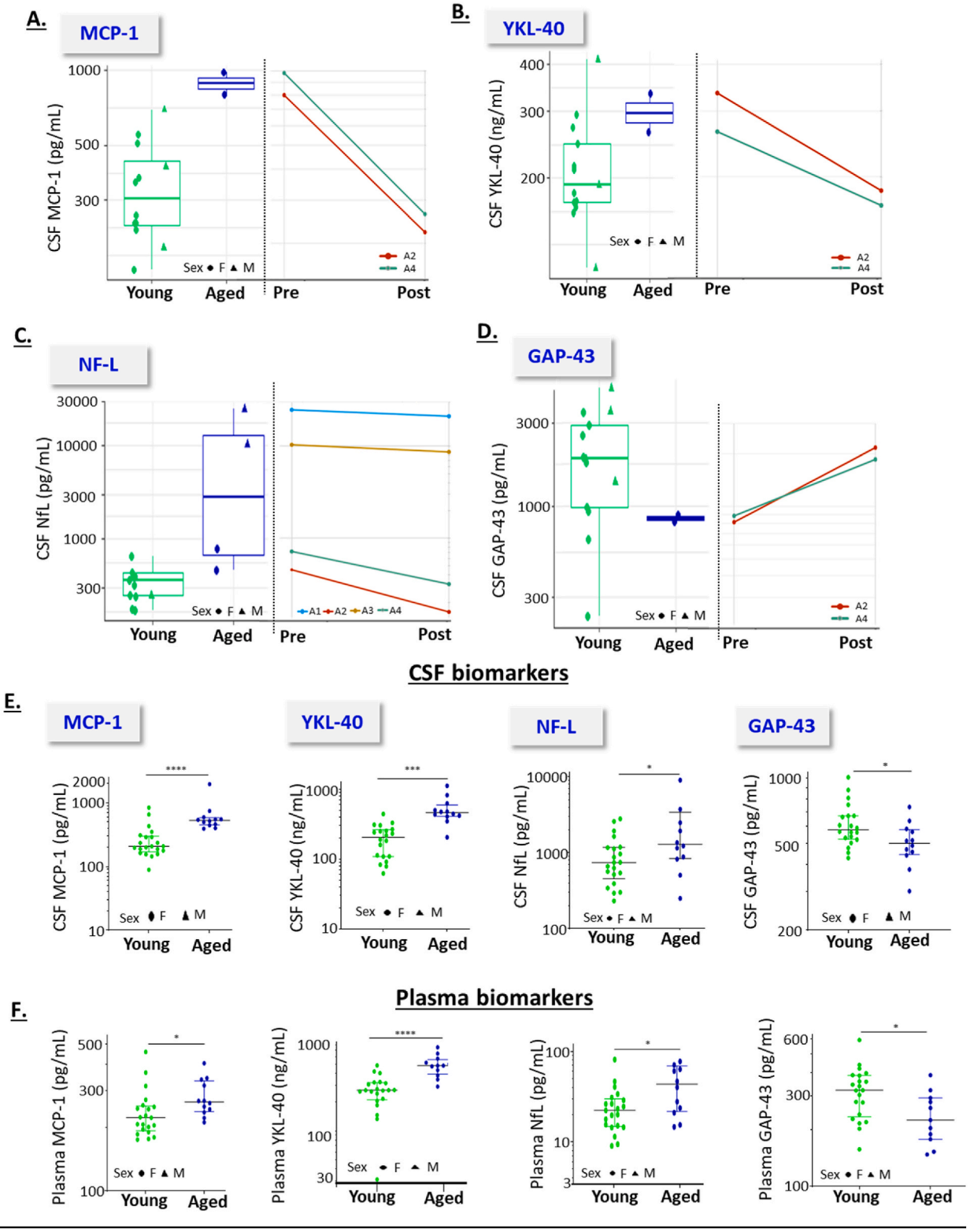

(caption on next page)

Fig. 4. Effect of age and Navitoclax on CSF biomarkers of SASP and neurodegeneration.
A.-D. Effect of age and navitoclax on CSF biomarkers. **A.** MCP-1. **B.** YKL-40. **C.** NF-L. **D.** GAP-43. *Left:* Baseline young (n = 12–13). *Right:* Effect of navitoclax on CSF biomarkers among individual aged NHP (n = 2–4). PRE: Baseline, samples collected after 1 cycle of low dose navitoclax lead-in (1.44 mg/kg). POST: post-navitoclax, samples collected 16 days after the last dose of navitoclax cycle 6. **E., F.** Baseline protein biomarkers of SASP and neurodegeneration in the CSF **(E.)** and plasma **(F.)** from a second cohort of young (N = 21) vs aged (N = 12). From left to right: MCP-1, YKL-40, NF-L, GAP-43 (a pre-synaptic protein biomarker to monitor synaptic health/synaptic damage). Error bars: ±1 SE. *p < 0.05, **p < 0.01, ***p < 0.001, ****p < 0.001. All statistical comparisons performed using Mann-Whitney test.

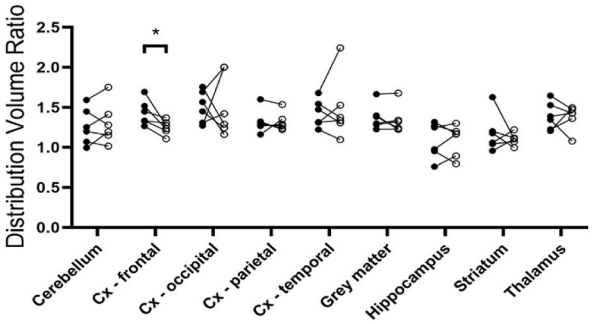

Fig. 5. Navitoclax effect on TSPO PET tracer binding in aged NHP.
TSPO-PET distribution volume ratios (DVR) for six aged NHPs before (closed symbol) and after navitoclax treatment (open symbol).

tolerability at therapeutic dosages in aged NHP, along with trends of reductions in biomarkers of senescence, SASP, neuroinflammation, and CNS damage, support further investigations of senolytics in clinical studies of neurodegenerative disorders.

Conflict of interest (or declarations) and funding

EFG, MV, AS, DRR, YZ, JQW, DWW, EA, MH, CH, RD, MT, KO, WA, LD, HK, JSS, YH, KM, VZ, SY, JM, YF, AV, SW, MD, SJF, and HF are employees of AbbVie and may hold stock. KD was an employee of AbbVie at the time of the study and may hold stock. The design, study conduct, and all funding for this research was provided by AbbVie, the maker of navitoclax (ABT-263). AbbVie participated in the interpretation of data, review, and approval of the publication. This study conforms to all ethical guidelines stated in Elsevier's Publishing Ethics Policy. The manuscript represents an accurate account of the work performed as well as an objective discussion of its significance. It consists of original work, with appropriate citations of publications influencing the reported work, and has not been published in other research journals. No generative AI or AI-assisted technologies were used in the creation of this manuscript.

Data availability

The data associated with this study has not been deposited into a publicly available repository; data will be made available on request.

CRediT authorship contribution statement

Edward F. Greenberg: Writing – review & editing, Writing – original draft, Visualization, Validation, Supervision, Methodology, Investigation, Formal analysis, Data curation, Conceptualization. **Martin J. Voorbach:** Writing – review & editing, Supervision, Resources, Project administration, Methodology, Investigation. **Alexandra Smith:** Writing – review & editing, Supervision, Resources, Investigation. **David R. Reuter:** Writing – review & editing, Methodology, Investigation, Data curation. **Yuchuan Zhuang:** Writing – review & editing, Methodology, Formal analysis, Data curation. **Ji-Quan Wang:** Methodology, Investigation, Formal analysis, Data curation. **Dustin W. Wooten:** Methodology, Investigation, Formal analysis, Data curation. **Elizabeth Asque:** Writing – review & editing, Visualization, Validation, Resources, Methodology, Investigation, Formal analysis, Data curation. **Min Hu:** Writing – review & editing, Visualization, Validation, Resources, Methodology, Investigation, Formal analysis, Data curation. **Carolin Hoft:** Writing – review & editing, Visualization, Validation, Supervision, Resources, Methodology, Investigation, Formal analysis, Data curation. **Ryan Duggan:** Writing – review & editing, Visualization, Resources, Methodology, Investigation, Formal analysis, Data curation. **Matthew Townsend:** Writing – review & editing, Validation, Resources, Methodology, Investigation, Formal analysis, Data curation. **Karin Orsi:** Writing – review & editing, Resources, Methodology, Investigation. **Karen Dalecki:** Writing – review & editing, Methodology, Investigation, Formal analysis, Data curation. **Willi Amberg:** Writing – review & editing, Methodology, Investigation, Formal analysis, Data curation. **Lori Duggan:** Writing – review & editing, Validation, Supervision, Methodology, Investigation, Formal analysis, Data curation. **Heather Knight:** Writing – review & editing, Resources, Methodology, Investigation, Formal analysis, Data curation. **Joseph S. Spina:** Writing – review & editing, Validation, Resources, Methodology, Investigation, Formal analysis, Data curation. **Yupeng He:** Writing – review & editing, Supervision, Resources, Methodology, Formal analysis. **Kennan Marsh:** Writing – review & editing,

Validation, Supervision, Resources, Project administration, Methodology, Investigation, Formal analysis, Data curation. **Vivian Zhao:** Writing – review & editing, Visualization, Validation, Resources, Methodology, Investigation, Formal analysis, Data curation. **Suzanne Ybarra:** Writing – review & editing, Resources, Project administration, Investigation, Data curation. **Jennifer Mollon:** Writing – review & editing, Visualization, Validation, Methodology, Formal analysis. **Yuni Fang:** Writing – review & editing, Validation, Supervision, Resources, Project administration, Investigation, Formal analysis, Data curation. **Aparna Vasanthakumar:** Writing – review & editing, Validation, Supervision, Resources, Methodology, Investigation, Formal analysis, Data curation. **Susan Westmoreland:** Writing – review & editing, Visualization, Supervision, Resources, Methodology, Investigation, Formal analysis, Data curation. **Mathias Droescher:** Writing – review & editing, Visualization, Validation, Supervision, Resources, Methodology, Investigation, Formal analysis, Data curation. **Sjoerd J. Finnema:** Writing – review & editing, Validation, Supervision, Resources, Methodology, Investigation, Formal analysis, Data curation, Conceptualization. **Hana Florian:** Writing – review & editing, Validation, Supervision, Resources, Methodology, Formal analysis, Conceptualization.

Declaration of competing interest

The authors declare the following financial interests/personal relationships which may be considered as potential competing interests:

Edward Greenberg, MD reports financial support was provided by AbbVie Inc. Edward Greenberg MD reports a relationship with AbbVie Inc that includes: employment, equity or stocks, and funding grants. EFG, MV, AS, DRR, YZ, JQW, DWW, EA, MH, CH, RD, MT, KO, WA, LD, HK, JSS, YH, KM, VZ, SY, JM, YF, AV, SW, MD, SJF, and HF are employees of AbbVie and may hold stock. KD was an employee of AbbVie at the time of the study and may hold stock. The design, study conduct, and all funding for this research was provided by AbbVie, the maker of navitoclax (ABT-263). AbbVie participated in the interpretation of data, review, and approval of the publication. If there are other authors, they declare that they have no known competing financial interests or personal relationships that could have appeared to influence the work reported in this paper.

Acknowledgements

The authors would like to thank former AbbVie colleagues Joel Leverson, Michael Gold, and Thomas Möller and current AbbVie colleagues Drs. Ole Graff, Tracey Posadas, Andy Souers, Kristine Gleason, Jalaja Potluri, Julie Adams, Julian Sefrin, Knut Biber, Eric Karran, Allison Thiede, Emily Voss, Jodi Ternes, Lynn Fojut, Monika Wood, Debra Weisbecker, Robert Dunstan, Terry Melim, and James Jasiek for helpful conversations, advice, and encouragement.

Appendix A. Supplementary data

Supplementary data to this article can be found online at https://doi.org/10.1016/j.heliyon.2024.e36483.

Abbreviations:

Aβ	Amyloid beta
AD	Alzheimer's Disease
ADAS-Cog	Alzheimer's Disease Assessment Scale-Cognitive subscale
ALS	Amyotrophic Lateral Sclerosis
APPPS1	Amyloid precursor protein/Presenilin Protein 1
Bcl-2	B-cell lymphoma 2
Bcl-xL:	B-cell lymphoma-extra large
β-actin	beta-actin
β2M	Beta-2 microglobulin
CD3	Cluster of Differentiation 3
CD14	Cluster of Differentiation 14
CD20	Cluster of Differentiation 20
CD56	Cluster of Differentiation 56
CDKN2A	Cyclin dependent kinase Inhibitor 2A, AKA p16
CDKN1A	Cyclin dependent kinase Inhibitor 1A, AKA p21
CHI3L1	Chitinase 3-like protein 1. AKA YKL-40
C_{max}	Maximum concentration achieved
CNS	Central nervous system
CSF	Cerebrospinal fluid
CWM	Cerebral White Matter
DQ	Dasatinib and Quercetin
DMT	Disease-modifying therapy
DVR	Distribution volume ratio
Ella	Ella automated immunoassay 600-100

EOT	End of Treatment
F_p:	Plasma free fraction
GAP-43	Growth associated protein 43
GFAP	Glial fibrillary acidic protein
H + L:	Heavy and light chain
H&E	Hematoxylin and eosin
HMGB1	High mobility group box protein 1
iADRS	Integrated Alzheimer's Disease Rating Scale
IHC	Immunohistochemistry
HRP	Horseradish Peroxidase
iADRS	Integrated Alzheimer's Disease Rating Scale
IL-1β	Interleukin-1 beta
IL-6	Interleukin 6
IL-8	Interleukin 8
LC3B	Microtubule-associated proteins 1A/1B light chain 3B
LMNB1	Lamin B1
MCP-1	Monocyte Chemoattractant Protein-1
mRNA	Messenger RNA
MS	Multiple Sclerosis
MSD	Meso Scale Discovery
NAV	Navitoclax
NF-L:	Neurofilament light
NFT	Neurofibrillary tangles
NHP	Non-human primate
p16	AKA CDKN2A
p21	AKA CDKN1A
p62	AKA Sequestosome-1 (SQSTM1)
PAI-1	Plasminogen Activator Inhibitor-1
PD	Parkinson's Disease
PFA	Paraformaldehyde
RT-PCR	Reverse Transcriptase Polymerase Chain Reaction
SA-β-gal	Senescence-associated beta galactosidase
SASP	Senescence Associated Secretory Phenotype
SC	Senescent cells
SE	Standard error
SIMOA	Single Molecule Array
SQSTM1	Sequestosome-1
sTREM2	Soluble triggering receptor expressed on myeloid cells 2
SMC	Single Molecule Counting
$t_{1/2}$	Half-life
TBS	Tris-buffered Saline
TNF-α:	Tumor necrosis factor alpha
TSPO-PET	Translocator Protein-Positron Emission Tomography
Vilip1	Visinin-like protein 1
V_T	Distribution volume
WT	Wild-type
YKL-40	Tyrosine lysine leucine-40 KDa. AKA Chitinase 3-like protein 1 (CHI3L1)

References

[1] J. Cummings, Y. Zhou, G. Lee, K. Zhong, J. Fonseca, F. Cheng, Alzheimer's disease drug development pipeline: 2023, Alzheimer's Dementia: Translational Research & Clinical Interventions 9 (2023) e12385.

[2] S.A. Beshir, A.M. Aadithsoorya, A. Parveen, S.S.L. Goh, N. Hussain, V.B. Menon, Aducanumab therapy to treat Alzheimer's disease: a narrative review, Int. J. Alzheimer's Dis. 2022 (2022) 9343514.

[3] C.T. Jack Cox, Biogen to Realign Resources for Alzheimer's Disease Franchise, Biogen news release, 2024.

[4] C.H. van Dyck, C.J. Swanson, P. Aisen, R.J. Bateman, C. Chen, M. Gee, M. Kanekiyo, D. Li, L. Reyderman, S. Cohen, L. Froelich, S. Katayama, M. Sabbagh, B. Vellas, D. Watson, S. Dhadda, M. Irizarry, L.D. Kramer, T. Iwatsubo, Lecanemab in early Alzheimer's disease, N. Engl. J. Med. 388 (2023) 9–21.

[5] Co L. Eisai, in: Topline Results of Clarity AD: Conference for Media and Investors, 2022.

[6] M.A. Mintun, A.C. Lo, C. Duggan Evans, A.M. Wessels, P.A. Ardayfio, S.W. Andersen, S. Shcherbinin, J. Sparks, J.R. Sims, M. Brys, L.G. Apostolova, S. P. Salloway, D.M. Skovronsky, Donanemab in early Alzheimer's disease, N. Engl. J. Med. 384 (2021) 1691–1704.

[7] G.M. Ashraf, N.H. Greig, T.A. Khan, I. Hassan, S. Tabrez, S. Shakil, I.A. Sheikh, S.K. Zaidi, M. Akram, N.R. Jabir, C.K. Firoz, A. Naeem, I.M. Alhazza, G. A. Damanhouri, M.A. Kamal, Protein misfolding and aggregation in Alzheimer's disease and type 2 diabetes mellitus, CNS Neurol. Disord.: Drug Targets 13 (2014) 1280–1293.

[8] A.B. Ganz, N. Beker, M. Hulsman, S. Sikkes, B. Netherlands Brain, P. Scheltens, A.B. Smit, A.J.M. Rozemuller, J.J.M. Hoozemans, H. Holstege, Neuropathology and cognitive performance in self-reported cognitively healthy centenarians, Acta Neuropathologica Communications 6 (2018) 64.

[9] T. Morawe, C. Hiebel, A. Kern, C. Behl, Protein homeostasis, aging and Alzheimer's disease, Mol. Neurobiol. 46 (2012) 41–54.

[10] J. Hwang, C.M. Estick, U.S. Ikonne, D. Butler, M.C. Pait, L.H. Elliott, S. Ruiz, K. Smith, K.M. Rentschler, C. Mundell, M.F. Almeida, N. Stumbling Bear, J. P. Locklear, Y. Abumohsen, C.M. Ivey, K.L.G. Farizatto, B.A. Bahr, The role of lysosomes in a broad disease-modifying approach evaluated across transgenic mouse models of Alzheimer's disease and Parkinson's disease and models of mild cognitive impairment, Int. J. Mol. Sci. 20 (2019).

[11] W. Wang, F. Zhao, X. Ma, G. Perry, X. Zhu, Mitochondria dysfunction in the pathogenesis of Alzheimer's disease: recent advances, Mol. Neurodegener. 15 (2020) 30.

[12] J.W. Kinney, S.M. Bemiller, A.S. Murtishaw, A.M. Leisgang, A.M. Salazar, B.T. Lamb, Inflammation as a central mechanism in Alzheimer's disease, Alzheimers Dement (N Y) 4 (2018) 575–590.

[13] P. Michalska, R. León, When it comes to an End: oxidative stress crosstalk with protein aggregation and neuroinflammation induce neurodegeneration, Antioxidants 9 (2020).

[14] P. Mao, P.H. Reddy, Aging and amyloid beta-induced oxidative DNA damage and mitochondrial dysfunction in Alzheimer's disease: implications for early intervention and therapeutics, Biochim. Biophys. Acta 1812 (2011) 1359–1370.

[15] L. Colnaghi, D. Rondelli, M. Muzi-Falconi, S. Sertic, Tau and DNA damage in neurodegeneration, Brain Sci. 10 (2020).

[16] N. Sabath, F. Levy-Adam, A. Younis, K. Rozales, A. Meller, S. Hadar, S. Soueid-Baumgarten, R. Shalgi, Cellular proteostasis decline in human senescence, Proc Natl Acad Sci U S A 117 (2020) 31902–31913.

[17] A. Meller, R. Shalgi, The aging proteostasis decline: from nematode to human, Exp. Cell Res. 399 (2021) 112474.

[18] M. Ogrodnik, S.A. Evans, E. Fielder, S. Victorelli, P. Kruger, H. Salmonowicz, B.M. Weigand, A.D. Patel, T. Pirtskhalava, C.L. Inman, K.O. Johnson, S. L. Dickinson, A. Rocha, M.J. Schafer, Y. Zhu, D.B. Allison, T. von Zglinicki, N.K. LeBrasseur, T. Tchkonia, N. Neretti, J.F. Passos, J.L. Kirkland, D. Jurk, Whole-body senescent cell clearance alleviates age-related brain inflammation and cognitive impairment in mice, Aging Cell 20 (2021) e13296.

[19] T.J. Bussian, A. Aziz, C.F. Meyer, B.L. Swenson, J.M. van Deursen, D.J. Baker, Clearance of senescent glial cells prevents tau-dependent pathology and cognitive decline, Nature 562 (2018) 578–582.

[20] T. Schilling, C. Eder, Microglial K+ channel expression in young adult and aged mice, Glia 63 (2015) 664–672.

[21] M. Abdouh, W. Chatoo, J. El Hajjar, J. David, J. Ferreira, G. Bernier, Bmi1 is down-regulated in the aging brain and displays antioxidant and protective activities in neurons, PLoS One 7 (2012) e31870.

[22] A.U. Joshi, P.S. Minhas, S.A. Liddelow, B. Haileselassie, K.I. Andreasson, G.W. Dorn, D. Mochly-Rosen, Fragmented mitochondria released from microglia trigger A1 astrocytic response and propagate inflammatory neurodegeneration, Nat. Neurosci. 22 (2019) 1635–1648.

[23] N. Musi, J.M. Valentine, K.R. Sickora, E. Baeuerle, C.S. Thompson, Q. Shen, M.E. Orr, Tau protein aggregation is associated with cellular senescence in the brain, Aging Cell 17 (2018) e12840.

[24] R. Bhat, E.P. Crowe, A. Bitto, M. Moh, C.D. Katsetos, F.U. Garcia, F.B. Johnson, J.Q. Trojanowski, C. Sell, C. Torres, Astrocyte senescence as a component of Alzheimer's disease, PLoS One 7 (2012) e45069.

[25] M. Xu, T. Pirtskhalava, J.N. Farr, B.M. Weigand, A.K. Palmer, M.M. Weivoda, C.L. Inman, M.B. Ogrodnik, C.M. Hachfeld, D.G. Fraser, J.L. Onken, K.O. Johnson, G.C. Verzosa, L.G.P. Langhi, M. Weigl, N. Giorgadze, N.K. LeBrasseur, J.D. Miller, D. Jurk, R.J. Singh, D.B. Allison, K. Ejima, G.B. Hubbard, Y. Ikeno, H. Cubro, V.D. Garovic, X. Hou, S.J. Weroha, P.D. Robbins, L.J. Niedernhofer, S. Khosla, T. Tchkonia, J.L. Kirkland, Senolytics improve physical function and increase lifespan in old age, Nat. Med. 24 (2018) 1246–1256.

[26] Y. Zhu, T. Tchkonia, T. Pirtskhalava, A.C. Gower, H. Ding, N. Giorgadze, A.K. Palmer, Y. Ikeno, G.B. Hubbard, M. Lenburg, S.P. O'Hara, N.F. LaRusso, J. D. Miller, C.M. Roos, G.C. Verzosa, N.K. LeBrasseur, J.D. Wren, J.N. Farr, S. Khosla, M.B. Stout, S.J. McGowan, H. Fuhrmann-Stroissnigg, A.U. Gurkar, J. Zhao, D. Colangelo, A. Dorronsoro, Y.Y. Ling, A.S. Barghouthy, D.C. Navarro, T. Sano, P.D. Robbins, L.J. Niedernhofer, J.L. Kirkland, The Achilles' heel of senescent cells: from transcriptome to senolytic drugs, Aging Cell 14 (2015) 644–658.

[27] Y. Zhu, T. Tchkonia, H. Fuhrmann-Stroissnigg, H.M. Dai, Y.Y. Ling, M.B. Stout, T. Pirtskhalava, N. Giorgadze, K.O. Johnson, C.B. Giles, J.D. Wren, L. J. Niedernhofer, P.D. Robbins, J.L. Kirkland, Identification of a novel senolytic agent, navitoclax, targeting the Bcl-2 family of anti-apoptotic factors, Aging Cell 15 (2016) 428–435.

[28] J. Chang, Y. Wang, L. Shao, R.-M. Laberge, M. Demaria, J. Campisi, K. Janakiraman, N.E. Sharpless, S. Ding, W. Feng, Y. Luo, X. Wang, N. Aykin-Burns, K. Krager, U. Ponnappan, M. Hauer-Jensen, A. Meng, D. Zhou, Clearance of senescent cells by ABT263 rejuvenates aged hematopoietic stem cells in mice, Nat. Med. 22 (2016) 78–83.

[29] M.P. Fatt, L.M. Tran, G. Vetere, M.A. Storer, J.V. Simonetta, F.D. Miller, P.W. Frankland, D.R. Kaplan, Restoration of hippocampal neural precursor function by ablation of senescent cells in the aging stem cell niche, Stem Cell Rep. 17 (2022) 259–275.

[30] P. Zhang, Y. Kishimoto, I. Grammatikakis, K. Gottimukkala, R.G. Cutler, S. Zhang, K. Abdelmohsen, V.A. Bohr, J. Misra Sen, M. Gorospe, M.P. Mattson, Senolytic therapy alleviates Aβ-associated oligodendrocyte progenitor cell senescence and cognitive deficits in an Alzheimer's disease model, Nat. Neurosci. 22 (2019) 719–728.

[31] M. Ebeling, E. Küng, A. See, C. Broger, G. Steiner, M. Berrera, T. Heckel, L. Iniguez, T. Albert, R. Schmucki, H. Biller, T. Singer, U. Certa, Genome-based analysis of the nonhuman primate Macaca fascicularis as a model for drug safety assessment, Genome Res. 21 (2011) 1746–1756.

[32] J.-M. Verdier, I. Acquatella, C. Lautier, G. Devau, S. Trouche, C. Lasbleiz, N. Mestre-Francés, Lessons from the analysis of nonhuman primates for understanding human aging and neurodegenerative diseases, Front. Neurosci. 9 (2015).

[33] U. Herbig, M. Ferreira, L. Condel, D. Carey, J.M. Sedivy, Cellular senescence in aging primates, Science 311 (2006), 1257-1257.

[34] J.C. Jeyapalan, M. Ferreira, J.M. Sedivy, U. Herbig, Accumulation of senescent cells in mitotic tissue of aging primates, Mech. Ageing Dev. 128 (2007) 36–44.

[35] E.S. Didier, A.G. MacLean, M. Mohan, P.J. Didier, A.A. Lackner, M.J. Kuroda, Contributions of nonhuman primates to research on aging, Veterinary Pathology 53 (2016) 277–290.

[36] R. Abdel Rassoul, S. Alves, V. Pantesco, J. De Vos, B. Michel, M. Perret, N. Mestre-Francés, J.-M. Verdier, G. Devau, Distinct transcriptome expression of the temporal cortex of the primate Microcebus murinus during brain aging versus Alzheimer's disease-like pathology, PLoS One 5 (2010) e12770.

[37] S.J. Chinta, G. Woods, M. Demaria, A. Rane, Y. Zou, A. McQuade, S. Rajagopalan, C. Limbad, D.T. Madden, J. Campisi, J.K. Andersen, Cellular senescence is induced by the environmental neurotoxin paraquat and contributes to neuropathology linked to Parkinson's disease, Cell Rep. 22 (2018) 930–940.

[38] K. Fujita, K. Motoki, K. Tagawa, X. Chen, H. Hama, K. Nakajima, H. Homma, T. Tamura, H. Watanabe, M. Katsuno, C. Matsumi, M. Kajikawa, T. Saito, T. Saido, G. Sobue, A. Miyawaki, H. Okazawa, HMGB1, a pathogenic molecule that induces neurite degeneration via TLR4-MARCKS, is a potential therapeutic target for Alzheimer's disease, Sci. Rep. 6 (2016) 31895.

[39] J.-P. Coppé, C.K. Patil, F. Rodier, Y. Sun, D.P. Muñoz, J. Goldstein, P.S. Nelson, P.-Y. Desprez, J. Campisi, Senescence-associated secretory phenotypes reveal cell-nonautonomous functions of oncogenic RAS and the p53 tumor suppressor, PLoS Biol. 6 (2008) e301.

[40] Y. Hu, G.L. Fryatt, M. Ghorbani, J. Obst, D.A. Menassa, M. Martin-Estebane, T.A.O. Muntslag, A. Olmos-Alonso, M. Guerrero-Carrasco, D. Thomas, M.S. Cragg, D. Gomez-Nicola, Replicative senescence dictates the emergence of disease-associated microglia and contributes to Aβ pathology, Cell Rep. 35 (2021).

[41] C.J.R. Fookes, T.Q. Pham, F. Mattner, I. Greguric, C. Loc'h, X. Liu, P. Berghofer, R. Shepherd, M.-C. Gregoire, A. Katsifis, Synthesis and biological evaluation of substituted [18F]Imidazo[1,2-a]pyridines and [18F]Pyrazolo[1,5-a]pyrimidines for the study of the peripheral benzodiazepine receptor using positron emission tomography, J. Med. Chem. 51 (2008) 3700–3712.

[42] J. Logan, J.S. Fowler, N.D. Volkow, G.-J. Wang, Y.-S. Ding, D.L. Alexoff, Distribution volume ratios without blood sampling from graphical analysis of PET data, J. Cerebr. Blood Flow Metabol. 16 (1996) 834–840.

[43] G. Serrano-Heras, I. Díaz-Maroto, B. Castro-Robles, B. Carrión, A.B. Perona-Moratalla, J. Gracia, S. Arteaga, F. Hernández-Fernández, J. García-García, O. Ayo-Martín, T. Segura, Isolation and quantification of blood apoptotic bodies, a non-invasive tool to evaluate apoptosis in patients with ischemic stroke and neurodegenerative diseases, Biol. Proced. Online 22 (2020) 17.

[44] F.J. Kohlhapp, D. Haribhai, R. Mathew, R. Duggan, P.A. Ellis, R. Wang, E.A. Lasater, Y. Shi, N. Dave, J.J. Riehm, V.A. Robinson, A.D. Do, Y. Li, C.J. Orr, D. Sampath, A. Raval, M. Merchant, A. Bhathena, A.H. Salem, K.M. Hamel, J.D. Leverson, C. Donawho, W.N. Pappano, T. Uziel, Venetoclax increases intratumoral effector T cells and antitumor efficacy in combination with immune checkpoint blockade, Cancer Discov. 11 (2021) 68–79.

[45] R.C. Team, R: A Language and Environment for Statistical Computing, R Foundation for Statistical Computing, Vienna, Austria, 2021.

[46] H. Wickham, ggplot2: Elegant Graphics for Data Analysis, Springer-Verlag, New York, 2016.

[47] E. Fielder, T. Wan, G. Alimohammadiha, A. Ishaq, E. Low, B.M. Weigand, G. Kelly, C. Parker, B. Griffin, D. Jurk, V.I. Korolchuk, T. von Zglinicki, S. Miwa, Short senolytic or senostatic interventions rescue progression of radiation-induced frailty and premature ageing in mice, Elife 11 (2022) e75492.

[48] M. Demaria, M.N. O'Leary, J. Chang, L. Shao, S. Liu, F. Alimirah, K. Koenig, C. Le, N. Mitin, A.M. Deal, S. Alston, E.C. Academia, S. Kilmarx, A. Valdovinos, B. Wang, A. de Bruin, B.K. Kennedy, S. Melov, D. Zhou, N.E. Sharpless, H. Muss, J. Campisi, Cellular senescence promotes adverse effects of chemotherapy and cancer relapse, Cancer Discov. 7 (2017) 165–176.

[49] J. Groh, K. Knöpper, P. Arampatzi, X. Yuan, L. Lößlein, A.-E. Saliba, W. Kastenmüller, R. Martini, Accumulation of cytotoxic T cells in the aged CNS leads to axon degeneration and contributes to cognitive and motor decline, Nature Aging 1 (2021) 357–367.

[50] D.A. Forero, Y. González-Giraldo, C. López-Quintero, L.J. Castro-Vega, G.E. Barreto, G. Perry, Meta-analysis of telomere length in Alzheimer's disease, J. Gerontol.: Series A 71 (2016) 1069–1073.

[51] T. Togo, H. Akiyama, E. Iseki, H. Kondo, K. Ikeda, M. Kato, T. Oda, K. Tsuchiya, K. Kosaka, Occurrence of T cells in the brain of Alzheimer's disease and other neurological diseases, J. Neuroimmunol. 124 (2002) 83–92.

[52] B.W. Dulken, M.T. Buckley, P. Navarro Negredo, N. Saligrama, R. Cayrol, D.S. Leeman, B.M. George, S.C. Boutet, K. Hebestreit, J.V. Pluvinage, T. Wyss-Coray, I. L. Weissman, H. Vogel, M.M. Davis, A. Brunet, Single-cell analysis reveals T cell infiltration in old neurogenic niches, Nature 571 (2019) 205–210.

[53] A. Sommer, B. Winner, I. Prots, The Trojan horse - neuroinflammatory impact of T cells in neurodegenerative diseases, Mol. Neurodegener. 12 (2017) 78.

[54] M. Althubiti, β2-microglobulin is overexpressed in buccal cells of elderly and correlated with expression of p16 and inflammatory genes, Saudi J. Biol. Sci. 29 (2022) 103418.

[55] M. Poblocka, A.L. Bassey, V.M. Smith, M. Falcicchio, A.S. Manso, M. Althubiti, X. Sheng, A. Kyle, R. Barber, M. Frigerio, S. Macip, Targeted clearance of senescent cells using an antibody-drug conjugate against a specific membrane marker, Sci. Rep. 11 (2021) 20358.

[56] X. Zhang, V.M. Pearsall, C.M. Carver, E.J. Atkinson, B.D.S. Clarkson, E.M. Grund, M. Baez-Faria, K.D. Pavelko, J.M. Kachergus, T.A. White, R.K. Johnson, C. S. Malo, A.M. Gonzalez-Suarez, K. Ayasoufi, K.O. Johnson, Z.P. Tritz, C.E. Fain, R.H. Khadka, M. Ogrodnik, D. Jurk, Y. Zhu, T. Tchkonia, A. Revzin, J. L. Kirkland, A.J. Johnson, C.L. Howe, E.A. Thompson, N.K. LeBrasseur, M.J. Schafer, Rejuvenation of the aged brain immune cell landscape in mice through p16-positive senescent cell clearance, Nat. Commun. 13 (2022) 5671.

[57] Z. Xu, A. Qu, H. Zhang, W. Wang, C. Hao, M. Lu, B. Shi, L. Xu, M. Sun, C. Xu, H. Kuang, Photoinduced elimination of senescent microglia cells in vivo by chiral gold nanoparticles, Chem. Sci. 13 (2022) 6642–6654.

[58] V. Budamagunta, A. Kumar, A. Rani, L. Bean, S. Manohar-Sindhu, Y. Yang, D. Zhou, T.C. Foster, Effect of peripheral cellular senescence on brain aging and cognitive decline, Aging Cell 22 (2023) e13817.

[59] J. Aguado, A.A. Amarilla, A. Taherian Fard, E.A. Albornoz, A. Tyshkovskiy, M. Schwabenland, H.K. Chaggar, N. Modhiran, C. Gómez-Inclán, I. Javed, A. A. Baradar, B. Liang, L. Peng, M. Dharmaratne, G. Pietrogrande, P. Padmanabhan, M.E. Freney, R. Parry, J.D.J. Sng, A. Isaacs, A.A. Khromykh, G. Valenzuela Nieto, A. Rojas-Fernandez, T.P. Davis, M. Prinz, B. Bengsch, V.N. Gladyshev, T.M. Woodruff, J.C. Mar, D. Watterson, E.J. Wolvetang, Senolytic therapy alleviates physiological human brain aging and COVID-19 neuropathology, Nature Aging 3 (2023) 1561–1575.

[60] N. Rachmian, S. Medina, U. Cherqui, H. Akiva, D. Deitch, D. Edilbi, T. Croese, T.M. Salame, J.M.P. Ramos, L. Cahalon, V. Krizhanovsky, M. Schwartz, Identification of senescent, TREM2-expressing microglia in aging and Alzheimer's disease model mouse brain, Nat. Neurosci 27 (2024) 1116–1124.

[61] A.D. Ruggiero, M. Block, M. Davis, R. Vemuri, M.E. Orr, K. Kavanagh, 753-P: senolytics improve diabetes measures in type 2 diabetic nonhuman primates: a pilot study, Diabetes 70 (2021).

[62] A.D. Ruggiero, R. Vemuri, M. Blawas, M. Long, D. DeStephanis, A.G. Williams, H. Chen, J.N. Justice, S.L. Macauley, S.M. Day, K. Kavanagh, Long-term dasatinib plus quercetin effects on aging outcomes and inflammation in nonhuman primates: implications for senolytic clinical trial design, GeroScience 45 (2023) 2785–2803.

[63] C.N. Harrison, J.S. Garcia, T.C.P. Somervaille, J.M. Foran, S. Verstovsek, C. Jamieson, R. Mesa, E.K. Ritchie, S.K. Tantravahi, P. Vachhani, C.L. O'Connell, R. S. Komrokji, J. Harb, J.E. Hutti, L. Holes, A.A. Masud, S. Nuthalapati, J. Potluri, N. Pemmaraju, Addition of navitoclax to ongoing ruxolitinib therapy for patients with myelofibrosis with progression or suboptimal response: phase II safety and efficacy, J. Clin. Oncol. 40 (2022) 1671–1680.

[64] C. Tse, A.R. Shoemaker, J. Adickes, M.G. Anderson, J. Chen, S. Jin, E.F. Johnson, K.C. Marsh, M.J. Mitten, P. Nimmer, L. Roberts, S.K. Tahir, Y. Xiao, X. Yang, H. Zhang, S. Fesik, S.H. Rosenberg, S.W. Elmore, ABT-263: a potent and orally bioavailable Bcl-2 family inhibitor, Cancer Res. 68 (2008) 3421–3428.

[65] M.E. Orr, A need for refined senescence biomarkers and measures of senolytics in the brain, J Alzheimers Dis 98 (2024) 411–415.

[66] W. He, X. Li, M. Morsch, M. Ismail, Y. Liu, F.U. Rehman, D. Zhang, Y. Wang, M. Zheng, R. Chung, Y. Zou, B. Shi, Brain-targeted codelivery of Bcl-2/Bcl-xl and Mcl-1 inhibitors by biomimetic nanoparticles for orthotopic glioblastoma therapy, ACS Nano 16 (2022) 6293–6308.

[67] E.G. Knox, M.R. Aburto, G. Clarke, J.F. Cryan, C.M. O'Driscoll, The blood-brain barrier in aging and neurodegeneration, Mol Psychiatry 27 (2022) 2659–2673.

[68] R. Gulej, Á. Nyúl-Tóth, C. Ahire, J. DelFavero, P. Balasubramanian, T. Kiss, S. Tarantini, Z. Benyo, P. Pacher, B. Csik, A. Yabluchanskiy, P. Mukli, A. Kuan-Celarier, I.A. Krizbai, J. Campisi, W.E. Sonntag, A. Csiszar, Z. Ungvari, Elimination of senescent cells by treatment with Navitoclax/ABT263 reverses whole brain irradiation-induced blood-brain barrier disruption in the mouse brain, Geroscience 45 (2023) 2983–3002.

[69] F.J. Padilla-Godínez, R. Ramos-Acevedo, H.A. Martínez-Becerril, L.D. Bernal-Conde, J.F. Garrido-Figueroa, M. Hiriart, A. Hernández-López, R. Argüero-Sánchez, F. Callea, M. Guerra-Crespo, Protein misfolding and aggregation: the relatedness between Parkinson's disease and hepatic endoplasmic reticulum storage disorders, Int. J. Mol. Sci. 22 (2021) 12467.

[70] L. McAlary, S.S. Plotkin, J.J. Yerbury, N.R. Cashman, Prion-like propagation of protein misfolding and aggregation in amyotrophic lateral sclerosis, Front. Mol. Neurosci. 12 (2019) 262, mediaalz.org 2020. Federal Alzheimer's and Dementia Research Funding Reaches $3.1 Billion Annually. Alzheimer's Association.

[71] M.A. David, M. Tayebi, Detection of protein aggregates in brain and cerebrospinal fluid derived from multiple sclerosis patients, Front. Neurol. 5 (2014) 251.

[72] B. Schattling, J.B. Engler, C. Volkmann, N. Rothammer, M.S. Woo, M. Petersen, I. Winkler, M. Kaufmann, S.C. Rosenkranz, A. Fejtova, U. Thomas, A. Bose, S. Bauer, S. Träger, K.K. Miller, W. Brück, K.E. Duncan, G. Salinas, P. Soba, E.D. Gundelfinger, D. Merkler, M.A. Friese, Bassoon proteinopathy drives neurodegeneration in multiple sclerosis, Nat. Neurosci. 22 (2019) 887–896.

[73] A. Höhn, A. Tramutola, R. Cascella, Proteostasis failure in neurodegenerative diseases: focus on oxidative stress, Oxid. Med. Cell. Longev. 2020 (2020) 5497046.

[74] Q. Wang, Y. Liu, J. Zhou, Neuroinflammation in Parkinson's disease and its potential as therapeutic target, Transl. Neurodegener. 4 (2015) 19.

[75] J. Liu, F. Wang, Role of neuroinflammation in amyotrophic lateral sclerosis: cellular mechanisms and therapeutic implications, Front. Immunol. 8 (2017) 1005.

[76] M.W. Psenicka, B.C. Smith, R.A. Tinkey, J.L. Williams, Connecting neuroinflammation and neurodegeneration in multiple sclerosis: are oligodendrocyte precursor cells a nexus of disease? Front. Cell. Neurosci. 15 (2021).

[77] S.J. Chinta, C.A. Lieu, M. Demaria, R.M. Laberge, J. Campisi, J.K. Andersen, Environmental stress, ageing and glial cell senescence: a novel mechanistic link to Parkinson's disease? J. Intern. Med. 273 (2013) 429–436.

[78] W. Oost, N. Talma, J.F. Meilof, J.D. Laman, Targeting senescence to delay progression of multiple sclerosis, J. Mol. Med. (Berl.) 96 (2018) 1153–1166.

[79] M. Kritsilis, V.R. S, P.N. Koutsoudaki, K. Evangelou, V.G. Gorgoulis, D. Papadopoulos, Ageing, cellular senescence and neurodegenerative disease, Int. J. Mol. Sci. 19 (2018).

[80] M.M. Das, C.N. Svendsen, Astrocytes show reduced support of motor neurons with aging that is accelerated in a rodent model of ALS, Neurobiol. Aging 36 (2015) 1130–1139.

[81] E. Trias, P.R. Beilby, M. Kovacs, S. Ibarburu, V. Varela, R. Barreto-Núñez, S.C. Bradford, J.S. Beckman, L. Barbeito, Emergence of microglia bearing senescence markers during paralysis progression in a rat model of inherited ALS, Front. Aging Neurosci. 11 (2019) 42.
[82] S.J. Miller, C.E. Campbell, H.A. Jimenez-Corea, G.H. Wu, R. Logan, Neuroglial senescence, α-synucleinopathy, and the therapeutic potential of senolytics in Parkinson's disease, Front. Neurosci. 16 (2022) 824191.
[83] I. Zanella, H. Blasco, M. Filosto, G. Biasiotto, Editorial: the impact of neurofilament light chain (NFL) quantification in serum and cerebrospinal fluid in neurodegenerative diseases, Front. Neurosci. 16 (2022).
[84] J.C. Masdeu, B. Pascual, M. Fujita, Imaging neuroinflammation in neurodegenerative disorders, J. Nucl. Med. 63 (2022) 45S.
[85] J. Hannestad, J.-D. Gallezot, T. Schafbauer, K. Lim, T. Kloczynski, E.D. Morris, R.E. Carson, Y.-S. Ding, K.P. Cosgrove, Endotoxin-induced systemic inflammation activates microglia: [11C]PBR28 positron emission tomography in nonhuman primates, Neuroimage 63 (2012) 232–239.
[86] A.T. Hillmer, D. Holden, K. Fowles, N. Nabulsi, B.L. West, R.E. Carson, K.P. Cosgrove, Microglial depletion and activation: a [11C]PBR28 PET study in nonhuman primates, EJNMMI Res. 7 (2017) 59.
[87] H. Tsukada, Effects of amyloid-β deposition on mitochondrial complex I activity in brain: a PET study in monkeys, in: INTECHOPEN (Ed.), Exploring New Findings on Amyloidosis, 2016.
[88] D.J. Baker, T. Wijshake, T. Tchkonia, N.K. LeBrasseur, B.G. Childs, B. van de Sluis, J.L. Kirkland, J.M. van Deursen, Clearance of p16Ink4a-positive senescent cells delays ageing-associated disorders, Nature 479 (2011) 232–236.
[89] M.M. Gonzales, V.R. Garbarino, E. Marques Zilli, R.C. Petersen, J.L. Kirkland, T. Tchkonia, N. Musi, S. Seshadri, S. Craft, M.E. Orr, Senolytic therapy to modulate the progression of Alzheimer's disease (SToMP-AD): a pilot clinical trial, J Prev Alzheimers Dis 9 (2022) 22–29.